10 dB Quantum-Enhanced Michelson Interferometer with Balanced Homodyne Detection

Joscha Heinze,* Karsten Danzmann, Benno Willke, and Henning Vahlbruch
Max-Planck-Institut für Gravitationsphysik (Albert-Einstein-Institut) and Leibniz Universität Hannover, 30167 Hannover, Germany

(Received 5 May 2022; accepted 10 June 2022; published 11 July 2022)

Future generations of gravitational-wave detectors (GWD) are targeting an effective quantum noise reduction of 10 dB via the application of squeezed states of light. In the last joint observation run O3, the advanced large-scale GWDs LIGO and Virgo already used the squeezing technology, albeit with a moderate efficiency. Here, we report on the first successful 10 dB sensitivity enhancement of a shot-noise limited tabletop Michelson interferometer via squeezed light in the fundamental Gaussian laser mode, where we also implement the balanced homodyne detection scheme that is planned for the third GWD generation. In addition, we achieved a similarly strong quantum noise reduction when the interferometer was operated in higher-order Hermite-Gaussian modes, which are discussed for the GWD thermal noise mitigation. Our results are an important step toward the targeted quantum noise level in future GWDs and, moreover, represent significant progress in the application of nonclassical states in higher-order modes for interferometry, increased spatial resolution, and multichannel sensing.

DOI: 10.1103/PhysRevLett.129.031101

The sensitivities of gravitational-wave detectors (GWDs) are limited by quantum noise over a broad frequency range. During the third joint observation run in 2019 and 2020, the Advanced LIGO and Virgo detectors mitigated the quantum shot noise effectively by about 3 dB via the injection of squeezed states of light into the detectors' output ports [1–4], and GEO600 could even demonstrate a shot-noise reduction of 6 dB [5]. However, this is still far below the 10 dB sensitivity enhancement that is targeted for the third generation of GWDs, the Einstein Telescope and Cosmic Explorer [6,7], and which could, so far, only be achieved in a tabletop Mach-Zehnder interferometer [8]. In contrast to the Michelson topology of GWDs, a Mach-Zehnder interferometer does not require a Faraday rotator (FR) unit for the injection of the squeezed field and, thus, implies significantly less optical loss. The highest reported quantum noise reduction including such an FR unit were 8.2 dB in a tabletop zero-area Sagnac interferometer [9].

At the moment, the GWDs Advanced LIGO, Advanced Virgo, KAGRA [10], and GEO600 employ the "dc readout" scheme. This is a special case of homodyne readout where the interferometer is stabilized to an offset from the dark fringe to provide a static local oscillator (LO) field. However, this technique includes several disadvantages, e.g., noise due to backscattering of the static LO field, or coupling of laser intensity as well as signal recycling cavity length fluctuations to the gravitational-wave readout due to the asymmetry of the operating arm cavities [6,11]. These disadvantages can be avoided by instead using the balanced homodyne readout scheme as proposed for the upgraded and third-generation detectors [6,7,12,13]. An investigation of the quantum noise reduction in the balanced homodyne detection topology is thus of high relevance.

Higher-order spatial modes offer a variety of benefits compared to the fundamental Gaussian $TEM_{0,0}$ mode owing to differences in their amplitude distributions. They have, for instance, been proposed for the thermal noise reduction in GWDs [14], to enhance the resolution in imaging techniques [15], to enable multichannel quantum communication and sensing [16], and to improve robustness against spatial mismatches [17,18]. If limited by quantum noise, these applications then naturally benefit from nonclassical states in the higher-order modes that could, however, not be efficiently realized so far.

Here, we combine the demonstration of unprecedented levels of quantum noise reduction ("squeezing levels") in a Michelson interferometer, including balanced homodyne readout, with the general proof of concept that a highly efficient quantum noise reduction is feasible in higher-order spatial mode applications.

Our setup as shown in Fig. 1 operates with a 2 W nonplanar ring laser (NPRO) that continuously emits light in the $TEM_{0,0}$ mode at a wavelength of 1064 nm. The major fraction of the light field is reflected toward the squeezed light source where the cavity-enhanced second harmonic generation (SHG) converts the incoming field to a wavelength of 532 nm to provide the pump field for the parametric down-conversion in a type-I optical parametric amplifier (OPA) [3,4]. The SHG is exclusively performed

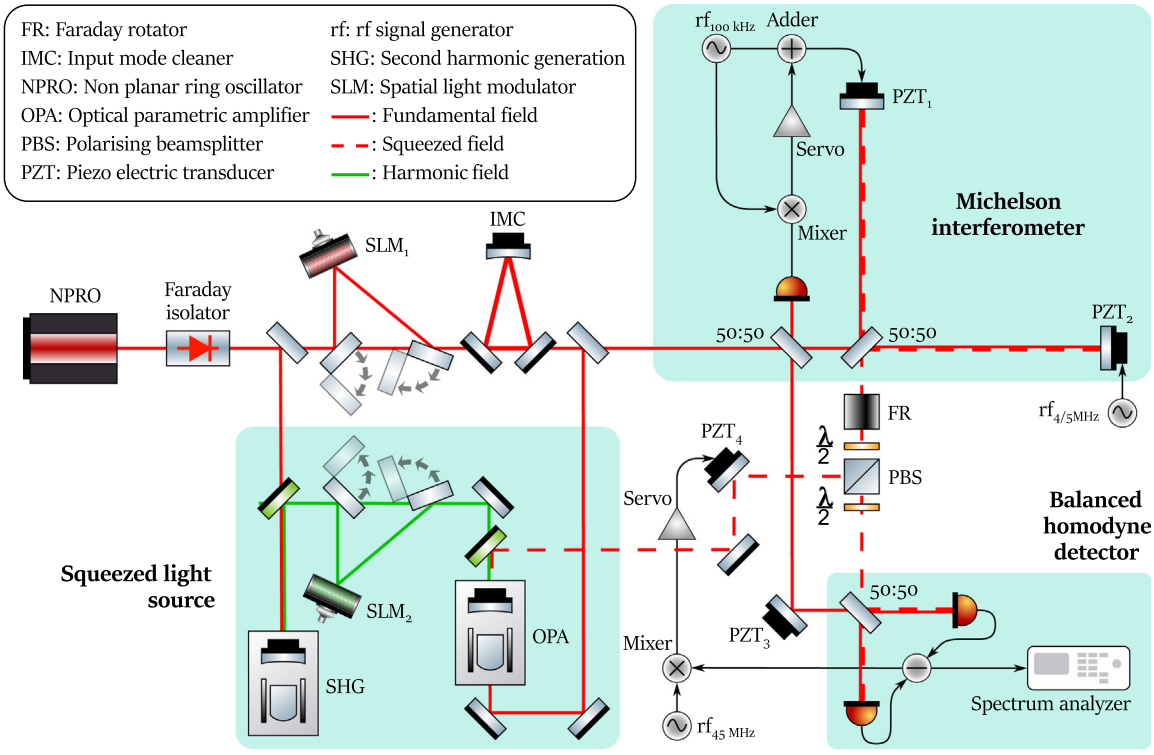

FIG. 1. Simplified schematic of the experimental setup.

in the $\mathrm{TEM}_{0,0}$ mode and the harmonic field then either bypasses the spatial light modulator SLM_2 or is converted into a higher-order pump mode via SLM_2 (see next paragraph) for a $\mathrm{TEM}_{0,0}$ or a higher-order mode operation of the OPA, respectively. The OPA cavity then generates squeezed states in the respective spatial mode of operation (SMOP) that are injected into the interferometer's output port.

For the mode conversion, we use one computer-controlled LCOS-Hamamatsu SLM for the fundamental and harmonic field each to convert the $\mathrm{TEM}_{0,0}$ mode into a higher-order spatial mode. These SLMs employ a liquid crystal that is divided into a fine transverse grid and whose orientation in each grid point can be actuated via an individual electric voltage, thereby controlling the individual optical path lengths. Hence, these SLMs impose a transverse phase distribution on the impinging beam for the mode conversion [19].

Our hemilithic linear OPA cavity contains a periodically poled potassium titanyl phosphate crystal with the dimensions $1.0 \times 2.0 \times 9.3$ mm in x, y, and z (propagation) direction. The highly reflective curved crystal face serves as the end mirror, $R_{\mathrm{end},1064\ \mathrm{nm}} > 99.96\%$ and $R_{\mathrm{end},532\ \mathrm{nm}} = 99.9\%$, while the plane face is antireflective coated for both wavelengths. The OPA's half-width at half maximum (bandwidth) is about 25 MHz and determined by the reflectivities of the incoupling mirror: $R_{\mathrm{in},1064\ \mathrm{nm}} = 92\%$ and $R_{\mathrm{in},532\ \mathrm{nm}} < 0.2\%$ (nominally). The radii of curvature are $R_{c,\mathrm{in}} = 25$ mm and $R_{c,\mathrm{end}} = 12$ mm such that the waist of the squeezed field's eigenmodes is about 33 μm in radius and located near the crystal center. A peltier element stabilizes the crystal temperature via a control loop and is used to optimize the phase matching. The SHG cavity has the same design besides a reflectivity of the incoupling mirror of $R_{\mathrm{in},1064\ \mathrm{nm}} = 90\%$. Further details on the squeezed light source can be found in [20].

The fraction of the 1064 nm field that is transmitted by the first mirror either bypasses SLM_1 to remain in the $\mathrm{TEM}_{0,0}$ mode or is converted by SLM_1 into the SMOP. The subsequent input mode cleaner (IMC) is stabilized to the resonance condition of the SMOP to provide a mode-filtered beam for a threefold downstream application. First, about 500 μW are reflected to the squeezed light source for the length stabilization of the OPA cavity to the resonance condition of the SMOP. Second, 7 mW are directly guided to the balanced homodyne detector as the local oscillator field. Third, 2 mW enter the interferometer through the input port. The Michelson interferometer consists of a 50:50 beamsplitter and two highly reflective end mirrors with attached piezoelectric transducers (PZT) and has an arm length of 10 cm. PZT_1 is driven at a radio frequency (rf) of 100 kHz and generates phase-modulation sidebands whose beat note with the carrier field is detected by the photo detector in reflection of the interferometer. We use the demodulated signal to stabilize the interferometer to the dark fringe with respect to the output port. PZT_2 can optionally inject a signal, which we will call the "GW signal" for the rest of this Letter. The frequency of this GW

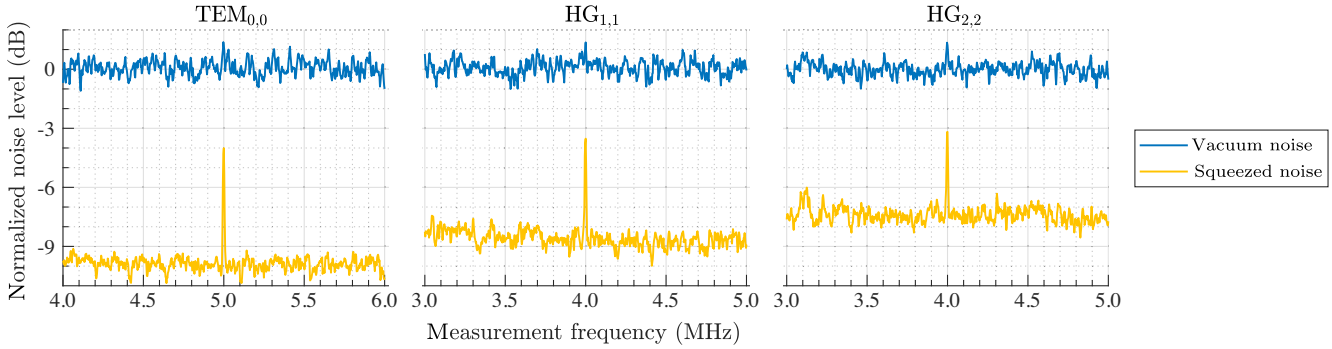

FIG. 2. Highest measured quantum noise reduction in the $TEM_{0,0}$, $HG_{1,1}$, and $HG_{2,2}$ mode with an injected GW signal. Resolution bandwidth: 10 kHz, video bandwidth: 10 Hz, electronic dark noise (not shown): about −22 dB and subtracted from the data. Antisqueezing levels (not shown): about 18 dB ($TEM_{0,0}$), 16 dB ($HG_{1,1}$), and 15 dB ($HG_{2,2}$).

signal is matched to the frequency where we observed the highest quantum noise reduction (4 MHz for the $HG_{1,1}$ and $HG_{2,2}$ mode and 5 MHz for the $TEM_{0,0}$ mode). The interferometer output field propagates to the balanced homodyne detector and is superimposed with the local oscillator field on a 50:50 beam splitter. We use PZT_3 to optimize the readout quadrature via the local oscillator phase for a maximum detected GW signal. A spectrum analyzer then measures the variance of the subtracted photo detector signals.

The combination of the polarizing beam splitter (PBS) and FR first injects the squeezed field into the interferometer and then transmits it toward the balanced homodyne detector after being effectively reflected by the interferometer. Phase-modulation sidebands, which remain in the squeezed field from the length stabilization of the OPA cavity, provide a 45 MHz beat note in the detector signal. We use this beat note to stabilize the relative phase between the squeezed and local oscillator field via PZT_4 for the controlled measurement of the squeezing and antisqueezing levels.

Figure 2 presents the measured variances of the interferometer output field in the signal (phase) quadrature with and without injected squeezed states ("squeezed noise" and "vacuum noise," respectively). We observed a maximum quantum shot-noise reduction of 10.0(0.3) db at a measurement frequency of 5 MHz and a harmonic OPA pump power of 55 mW in the $TEM_{0,0}$ mode. At a measurement frequency of 4 MHz, we achieved 8.8(0.3) dB at a pump power of 550 mW and 7.5(0.3) dB at a pump power of 800 mW in the $HG_{1,1}$ and $HG_{2,2}$ mode, respectively. In each case, the injected GW signal had an amplitude of about −5.3 dB and could hardly be detected in the vacuum state related noise floor. However, it appears as a distinct peak in the squeezed state related noise curves. The significant differences in the required pump power mainly arise due to the imperfect generation of the unfiltered pump field with SLM_2 whose conversion efficiency is most likely below 30%. In addition, the pump efficiency fundamentally decreases with increasing mode order. Further details can be found in [20].

In our setup, three main factors limit the squeezing level: the detection efficiency, the phase noise, and the technical laser noise [21]. The first is a combined effect from the OPA escape efficiency, loss from optics in the path of the squeezed field, the homodyne contrast between the local oscillator and squeezed field, and the detector's quantum efficiency (see Table I). Among the optics in the squeezed beam path, the Faraday rotator in combination with the PBS causes the highest loss, which amounted to about 1%–1.5% per single pass and increased with the mode order due to additional clipping loss (aperture radius: about 2.5 mm, beam radius: about 1 mm). Furthermore, the imperfect homodyne contrast includes several influences: beam misalignments and mismatches in the waist size and position are always present in practice and cause a larger reduction in the homodyne contrast with increasing mode order [22]; possible rotations around the optical axis can reduce the contrast for the higher-order HG modes, and mode degeneracies are also potentially more severe for the higher-order modes [23]. While the reduction in the homodyne contrast was not resolved with respect to these causes, the differences can theoretically be explained by the first alone. Specific issues with rotations or degeneracies were not

TABLE I. Measured optical loss budget, the expected detection efficiency, and the measured interferometer contrast [interferometer (IFO)].

Optical loss source	$TEM_{0,0}$	$HG_{1,1}$	$HG_{2,2}$
OPA escape efficiency (%)	1.0(5)	1.0(5)	1.0(5)
Squeezed beam path optics (%)	3.0(5)	4.0(5)	4.5(5)
Leakage to IFO input port (%)	0.3(1)	0.3(1)	0.4(1)
Homodyne contrast (%)	2.2(6)	2.8(6)	6.0(6)
Detector quantum efficiency (%)	0.7(4)	0.7(4)	0.7(4)
Expected detection efficiency (%)	92.8(10)	91.2(10)	87.4(10)
Fitted detection efficiency (%)	92.6(10)	91.4(10)	87.7(10)
Maximum IFO contrast (%)	99.92(2)	99.87(2)	99.74(2)
IFO leakage power (μW)	5(2)	6(2)	8(2)

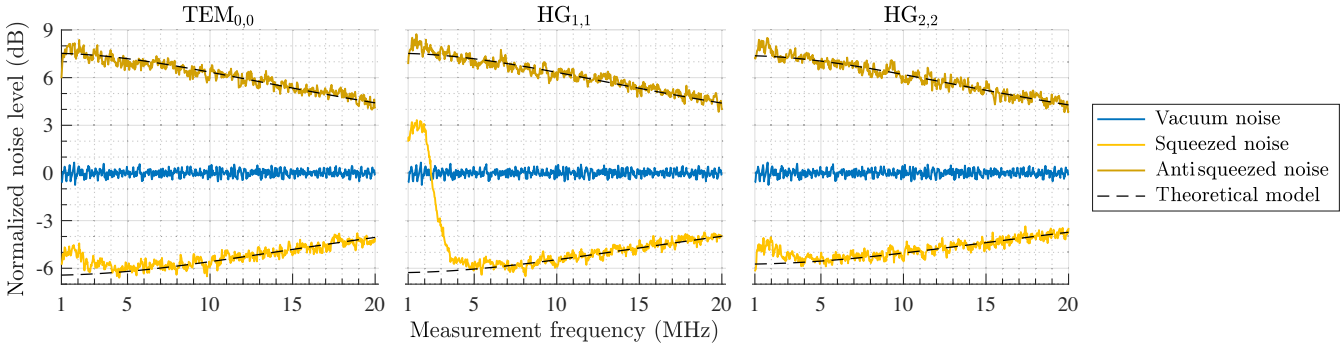

FIG. 3. Variances of the quantum noise for the $TEM_{0,0}$, $HG_{1,1}$, and $HG_{2,2}$ mode for low levels of antisqueezing and no injected GW signal. The results correspond to a harmonic OPA pump power of about 10, 100, and 150 mW, respectively. Resolution bandwidth: 300 kHz, video bandwidth: 300 Hz, electronic dark noise (not shown): about −22 dB and subtracted from the data.

observed. The second factor, phase noise, reduces the squeezing level due to fluctuations in the relative phase between the LO and squeezed field, especially in the regime of high antisqueezing. The third factor becomes relevant due to the coherent amplitude in the detected field that arises from the interfering coherent amplitudes in the residual OPA control field and the interferometer leakage field. The latter results from an imperfect interferometer contrast, which depends on the SMOP and is indicated in Table I, and an unintended but possible small dark fringe offset. We measured the coherent power in the OPA control field to be about 2 μW, SMOP-independently. The measured power in the interferometer leakage field is indicated in Table I. The leakage power is highly sensitive to the interferometer alignment, i.e., the effective contrast, and varied by 25% to 40% over time.

In a separate measurement run with different power levels injected into the interferometer input port, we could confirm that the total detected technical laser noise significantly limited the squeezing level up to a measurement frequency of about 5 MHz. This was most relevant for the $TEM_{0,0}$ measurement as it limited the quantum noise reduction at 4 MHz to below 10 dB, thereby shifting the frequency of the maximum observed quantum noise reduction from 4 to 5 MHz compared to the $HG_{1,1}$ and $HG_{2,2}$ mode. In addition, the coherent amplitude in the detected field slightly reduces the squeezing level over the whole frequency band because it beats with the vacuum fluctuations entering from the local oscillator port of the detector. This leads to an effective pseudo-dark noise floor—when only the local oscillator port of the detector is blocked—that we typically observed to be 1 to 2 dB above the actual electronic dark noise—when both detector input ports are blocked. We only subtracted the actual electronic dark noise in all presented measurements. With the technical laser noise and the amplification of the LO field's vacuum fluctuations, the reduction in the squeezing level due to the coherent amplitude in the detected field dominates and covers the effect of phase noise. The latter can, thus, not be conclusively inferred for our setup.

To check the expected detection efficiencies against the measurement data without a significant disturbance from either technical laser or phase noise, we compare squeezing and antisqueezing levels at low harmonic OPA pump power and up to a measurement frequency of 20 MHz with a theoretical model (see Fig. 3). Below threshold and without phase noise, the detected squeezed (−) and antisqueezed (+) quadrature variances of the OPA output field can be computed as [24]

$$\Delta^2 \hat{X}_{+,-} = 1 \pm \eta_{\mathrm{det}} \frac{4\sqrt{P/P_{\mathrm{thr}}}}{(1 \mp \sqrt{P/P_{\mathrm{thr}}})^2 + 4(\frac{2\pi f}{\gamma})^2}, \quad (1)$$

where η_{det} is the detection efficiency, P is the harmonic pump power, P_{thr} is the threshold power, f is the measurement frequency, and $\gamma = c(T + L)/l$ is the cavity decay rate with the speed of light c, the incoupling mirror's power transmissivity T of the OPA cavity, the round-trip loss L and the round-trip optical path length l. The parameters η_{det} and P_{thr} can then be varied until the optimum match between the model and the measurement data is obtained (dashed lines in Fig. 3). The derived values for the detection efficiencies are indicated in Table I and agree well with our expectations. The characteristics of the technical laser noise can be identified in the squeezed noise of each mode at low frequencies, where the noise peak in the $HG_{1,1}$ measurement was atypically large and affected the squeezing level up to a frequency of 6 MHz. This $HG_{1,1}$ measurement was prepared with the same care as the others and shows how sensitive the setup is with respect to the interferometer alignment and resulting leakage power. The preparation procedure for each measurement was done in the following order: adjusting the interferometer contrast via the PZT_1 and PZT_2 mirrors, adjusting the alignment between the squeezed field and coherent interferometer field via mirrors around PZT_4, adjusting the alignment between the squeezed field from the north arm and the LO field via mirrors around PZT_3, and adjusting the alignment between the squeezed field from the east arm and the LO field via

PZT_2. For the $HG_{1,1}$ measurement in Fig. 3, the last step may have reduced the interferometer contrast unintentionally. We show it for demonstration purposes.

In conclusion, we reported on the first 10 dB squeezed-light enhancement of a shot-noise limited Michelson interferometer, here demonstrated in a tabletop balanced homodyne detection topology. While we achieved this result in the $TEM_{0,0}$ mode, we as well reached strong sensitivity enhancements of close to 9 dB and 7.5 dB in the $HG_{1,1}$ and $HG_{2,2}$ modes, respectively. In our experiment, optical loss from the Faraday rotator unit that couples the squeezed light into the interferometer and loss associated with the homodyne contrast primarily limited the detection efficiency for the squeezed light. Technical laser noise, which becomes relevant due to a coherent amplitude in the detected field, further reduced the squeezing level below measurement frequencies of 5 MHz and also affected the frequency at which the highest quantum noise reduction was observed. These results are an important prototype demonstration for future gravitational-wave detectors and represent a milestone for the efficient usage of nonclassical states of light in higher-order modes in a measurement application.

Funded by the Deutsche Forschungsgemeinschaft (DFG, German Research Foundation) under Germany's Excellence Strategy—EXC-2123 QuantumFrontiers—390837967.

*Corresponding author.
joscha.heinze@aei.mpg.de

[1] A. Buikema *et al.*, Sensitivity and performance of the Advanced LIGO detectors in the third observing run, Phys. Rev. D **102**, 062003 (2020).

[2] D. Bersanetti, B. Patricelli, O. J. Piccinni, F. Piergiovanni, F. Salemi, and V. Sequino, Advanced Virgo: Status of the detector, latest results and future prospects, Universe **7**, 322 (2021).

[3] M. Tse *et al.*, Quantum-Enhanced Advanced LIGO Detectors in the Era of Gravitational-Wave Astronomy, Phys. Rev. Lett. **123**, 231107 (2019).

[4] M. Mehmet and H. Vahlbruch, The squeezed light source for the Advanced Virgo detector in the observation run O3, Galaxies **8**, 79 (2020).

[5] J. Lough, E. Schreiber, F. Bergamin, H. Grote, M. Mehmet, H. Vahlbruch, C. Affeldt, M. Brinkmann, A. Bisht, V. Kringel, H. Lück, N. Mukund, S. Nadji, B. Sorazu, K. Strain, M. Weinert, and K. Danzmann, First Demonstration of 6 dB Quantum Noise Reduction in a Kilometer Scale Gravitational Wave Observatory, Phys. Rev. Lett. **126**, 041102 (2021).

[6] ET Steering Committee, ET design report update 2020 (2020), http://www.et-gw.eu/index.php/relevant-et-documents (accessed: 2022-04-02).

[7] D. Reitze, R. X. Adhikari, S. Ballmer, B. Barish, L. Barsotti, G. Billingsley, A. D. Brown, Y. Chen, D. Coyne, R. Eisenstein *et al.*, Cosmic Explorer: The U.S. contribution to gravitational-wave astronomy beyond LIGO, Bull. AAS **51**, 035 (2019), https://baas.aas.org/pub/2020n7i035/release/1.

[8] J. Zander, Squeezed and entangled light: From foundations of quantum mechanics to quantum sensing, Ph.D. thesis, Universität Hamburg, 2021, https://ediss.sub.uni-hamburg.de/handle/ediss/9171.

[9] T. Eberle, S. Steinlechner, J. Bauchrowitz, V. Händchen, H. Vahlbruch, M. Mehmet, H. Müller-Ebhardt, and R. Schnabel, Quantum Enhancement of the Zero-Area Sagnac Interferometer Topology for Gravitational Wave Detection, Phys. Rev. Lett. **104**, 251102 (2010).

[10] T. Akutsu *et al.*, Overview of KAGRA: Detector design and construction history, Prog. Theor. Exp. Phys. **2021**, 125 (2020).

[11] P. Fritschel, M. Evans, and V. Frolov, Balanced homodyne readout for quantum limited gravitational wave detectors, Opt. Express **22**, 4224 (2014).

[12] H. Yu, D. Martynov, S. Vitale, M. Evans, D. Shoemaker, B. Barr, G. Hammond, S. Hild, J. Hough, S. Huttner, S. Rowan, B. Sorazu, L. Carbone, A. Freise, C. Mow-Lowry, K. L. Dooley, P. Fulda, H. Grote, and D. Sigg, Prospects for Detecting Gravitational Waves at 5 Hz with Ground-Based Detectors, Phys. Rev. Lett. **120**, 141102 (2018).

[13] R. X. Adhikari *et al.*, A cryogenic silicon interferometer for gravitational-wave detection, Classical Quantum Gravity **37**, 165003 (2020).

[14] J.-Y. Vinet, Thermal noise in advanced gravitational wave interferometric antennas: A comparison between arbitrary order Hermite and Laguerre Gaussian modes, Phys. Rev. D **82**, 042003 (2010).

[15] N. Uribe-Patarroyo, A. Fraine, D. S. Simon, O. Minaeva, and A. V. Sergienko, Object Identification Using Correlated Orbital Angular Momentum States, Phys. Rev. Lett. **110**, 043601 (2013).

[16] M. Lassen, V. Delaubert, J. Janousek, K. Wagner, H.-A. Bachor, P. K. Lam, N. Treps, P. Buchhave, C. Fabre, and C. C. Harb, Tools for Multimode Quantum Information: Modulation, Detection, and Spatial Quantum Correlations, Phys. Rev. Lett. **98**, 083602 (2007).

[17] C. Roh, G. Gwak, and Y.-S. Ra, Robust squeezed light against mode mismatch using a self imaging optical parametric oscillator, Sci. Rep. **11**, 18991 (2021).

[18] S. Steinlechner, N.-O. Rohweder, M. Korobko, D. Töyrä, A. Freise, and R. Schnabel, Mitigating Mode-Matching Loss in Nonclassical Laser Interferometry, Phys. Rev. Lett. **121**, 263602 (2018).

[19] S. Ast, S. Di Pace, J. Millo, M. Pichot, M. Turconi, N. Christensen, and W. Chaibi, Higher-order Hermite-Gauss modes for gravitational waves detection, Phys. Rev. D **103**, 042008 (2021).

[20] J. Heinze, B. Willke, and H. Vahlbruch, Observation of Squeezed States of Light in Higher-Order Hermite-Gaussian Modes with a Quantum Noise Reduction of up to 10 dB, Phys. Rev. Lett. **128**, 083606 (2022).

[21] S. Steinlechner, B. W. Barr, A. S. Bell, S. L. Danilishin, A. Gläfke, C. Gräf, J.-S. Hennig, E. A. Houston, S. H. Huttner,

S. S. Leavey, D. Pascucci, B. Sorazu, A. Spencer, K. A. Strain, J. Wright, and S. Hild, Local-oscillator noise coupling in balanced homodyne readout for advanced gravitational wave detectors, Phys. Rev. D **92**, 072009 (2015).

[22] L. Tao, J. Kelley-Derzon, A. C. Green, and P. Fulda, Power coupling losses for misaligned and mode-mismatched higher-order Hermite–Gauss modes, Opt. Lett. **46**, 2694 (2021).

[23] L. Tao, A. Green, and P. Fulda, Higher-order Hermite-Gauss modes as a robust flat beam in interferometric gravitational wave detectors, Phys. Rev. D **102**, 122002 (2020).

[24] E. S. Polzik, J. Carri, and H. J. Kimble, Atomic spectroscopy with squeezed light for sensitivity beyond the vacuum-state limit, Appl. Phys. B **55**, 279 (1992).